RSC Advances

ROYAL SOCIETY OF CHEMISTRY

www.rsc.org/advances

Microwave synthesis of $CoSe_2$/graphene-TiO_2 heterostructure for improved hydrogen evolution from aqueous solution in the presence of sacrificial agents

Kefayat Ullah, Zhu lei, Shu Ye, Asghar Ali, Won-Chun Oh*

Department of Advanced Materials Science & Engineering, Hanseo University, Seosan-si, Chungnam-do, Korea, 356-706

Abstract:

Heterogeneous material consisting of tube type TiO_2 was grown in the presence of $CoSe_2$/graphene hybrid as a high-performance photocatalyst material through fast microwave assisted technique. The prepared composites were characterized by X-ray diffraction (XRD), scanning electron microscopy (SEM), transmission electron microscopy (TEM), Raman spectroscopic analysis, UV-vis absorbance spectra and UV-vis diffuse reflectance spectra (DRS) analysis were obtained. The hydrogen evolution rate for ternary composites was found markedly high as compare to bare TiO_2 and binary $CoSe_2$/graphene composites. This extraordinary photocatalytic activity for hydrogen evolution arises from the positive synergetic effect between the $CoSe_2$ and graphene components in our heterogeneous system. The optical properties were also observed to be effected by the different weight % of graphene in the composites by observing their respective band gaps from DRS spectra.

Key words: Microwave; Raman; nanocomposite; DRS, hydrogen evolution

* Corresponding author
E-mail: wc_oh@hanseo.ac.kr
Tel: +82-41-660-1337, Fax:+82-41-688-3352

1. Introduction:

Hydrogen production from water splitting through graphene based semiconductor photocatalyst has attracted amassing attention in the past due to its great potential in obtaining renewable energy [1]. Heterogeneous catalyst system consists of two semiconductor materials and mediator/support material or the class of photocatalyst for solar hydrogen production. The significant advantage of the heterogeneous systems is the separation of photoexcited electrons and holes with strong redox potentials on different semiconductors. So for in these systems a new reversible donor/acceptor pair as redox mediator was introduced in the reaction solution to facilitate the charge transfer between two semiconductor materials. These mediators are mainly (Fe^3, Fe^2, IO^3 *etc*, [2-5]. Similarly a solid state electron mediator was also introduced to reduce the backward reduction involving redox mediator [6-7]. The introduction of these metallic components as electron mediator has several draw backs involving high price, metallic pollution, corrosion etc. Therefore a suitable electron mediator was needed to design a new heterogeneous system for improved catalytic effect towards hydrogen production.

Recently graphene has been used very extensively to combine with various semiconductor materials. The surface functionalities, large surface area and stability of graphene make it a suitable candidate to ensure the attachment of semiconductor materials on its surface and facilitate the charge transfer mechanism. The oxygen functionalities affect the particle size and shape of the guest material on graphene sheet. The guest materials properties and shape are very important in photocatalyst mechanism system. The surface modifications of graphene through these semiconductor materials open up new ways to establish and design semiconductor photocatalyst with desire properties.

Several scientists have already reported that graphene can act as photosensitizer to extend the light response or it can reduce the band gap of wide semiconductor such as TiO_2, ZnO towards the visible range of electromagnetic spectrum [8-9]. Recently, a special attention has been paid to coupled graphene/TiO_2 system due to high surface area and excellent charge conductivity of graphene and nontoxicity, low price and environmental friendly behavior of TiO_2 [10-12]. It was observed that graphene can effectively transfer and store excited electron when coupled with TiO_2 semiconductor. Due to π-π interaction it can also enhance the affinity with organic pollutant and can help to enhance the catalytic process. The fabrication of new photocatalyst needs a special attention to meet the environmental requirements. i.e., the stability, nontoxicity, simple

and fast synthesis techniques. Heterogeneous photocatalyst system can produce better catalytic activity due to the synergistic effect between two of them. The energy level of the system can be adjusted to desire level by quantum confinements. The transfer of electrons in the heterogeneous system between two catalysts is the main feature for the production of H_2 or other mineral products. The main challenge in these systems is the introduction of electron mediator with stable conducting properties and having great interfacial contact [31-14].

Inspite of these promising properties the main problem in ternary system is the agglomeration of nanoparticle on graphene sheet due to large number of functional groups on graphene surface. These agglomeration lead towards lower surface area and poor interfacial contact. Therefore homogenous distribution of nanoparticles, high surface area and better interfacial contact are the requirements of ternary photocatalyst materials [15].

In this work we report a fast and facile route for the preparation of a $CoSe_2$/graphene supported TiO_2 photocatalyst through microwave-assisted techniques. In this process, cobalt acetate and selenium salt were mixed together in 100 ml ethylene glycol followed by graphene oxide, the resulting solution is irradiated by microwaves for 300 s followed by mixing of TiO_2 precursor material under appropriate conditions. During microwave irradiation, partial reduction of graphene oxide into graphene and attachment of $CoSe_2$ nanoparticles and TiO_2 nanotubes on graphene sheets was observed in ethylene glycol. The photocatalytic activities of as-prepared nanocomposites were tested for the production of hydrogen from aqueous solution containing Na_2So_3/Na_2S and methanol as sacrificial reagents.

2. Experimental section

2.1. Materials

Titanium (IV) n-butoxide (TNB, $C_{16}H_{36}O_4Ti$) used as a titanium precursor was purchased from Samchun Pure Chemical Co. Ltd., Korea. Selenium powder (Se, 99%) and ammonium hydroxide (NH_4OH, 25–28) were purchased from Daejung Chemicals Co. Ltd., Korea, Sodium sulfide pentahydrate ($Na_2S.5H_2O$) and sodium sulfite (Na_2SO_3) were purchased from Samchun Pure Chemical Co. Ltd, Korea. Cobalt chloride ($CoCl_2$) was purchased from Dae-Jung Chemicals & Metal Co., Ltd., Korea. Ethylene glycol was purchased from Dae-Jung Chemical and Metals Co. Ltd Korea. All chemicals were used without further purification and all experiments were carried out using distilled water.

2.2. Synthesis of Cobalt Selenide

Cobalt selenide was synthesized through fast microwave assisted techniques. In a typical synthesis, 1.5 g of anhydrous sodium sulfite (Na_2SO_3) and 0.3 g of crude selenium (Se) powder were mixed together in 300 ml ethylene glycol under vigorous magnetic stirring. The solution was stirred vigorously for 1 h at 50 °C to ensure homogeneous mixture to achieve selenium. In the next step 0.5 mmol of cobalt acetate was added to the above solution and stirred for 20 minutes to attain a stable solution. The obtained solution was finally transferred to a 500 ml reaction vessel and placed in a conventional microwave oven. The solution was then irradiated with microwaves for 300 s, with periodic on offsetting after 5 s. The mixture was then cooled to room temperature, filtered with Whatman filter paper and heat treated for 5 h at 90 °C to obtain a dark brown $CoSe_2$ powder.

2.3. Synthesis of $CoSe_2$/graphene Nanocomposites

The GO were prepared through modified Hoffman method reported elsewhere [16]. GO (200 mg) were dispersed in ethylene glycol (EG) solution (100 mL) under vigorous stirring to form a solution A. Cobalt selenide was prepared as explain above. 0.9 molar solution of cobalt selenide was prepared to form a solution B. A and B were mixed together stirred for several minutes and transferred into a 500 mL reaction vessel placed in a conventional microwave oven. The solution is then irradiated with microwave for 5 sec on and 5 sec off for 300 seconds, and cooled at room temperature filtered with whatman filter paper. The resultant powder was washed 3 times with distilled water and transferred into a dry oven for 6 hours at 90 ^oC. The powder was then heat treated at 500 ^oC for 1 hr in electric furnace. The sample obtained was labeled as $CoSe_2$-G nanocomposites.

2.4. Synthesis of $CoSe_2$/graphene-TiO_2 nanocomposites

$CoSe_2$/graphene-TiO_2 nanocomposites were obtained by following the above method. A borosilicate glass sealed reaction vessel specially designed for microwave techniques having a diameter of 8 cm and height 10 cm was used. Graphene oxide 200 mg and desired amount of TNB as titanium precursor was dispersed in 300 ml ethylene glycol for 30 minutes to attain a homogenous mixture to form a solution A. In the next step 1 g of anhydrous sodium sulfite (Na_2SO_3) and 0.2 g of crude selenium powder (Se) were vigorously stirred in 200 mL of ethylene glycol for 30 min to attain a homogenous solution. Followed by the addition of desired amount of cobalt acetate with vigorous stirring for 1 h at 35 ^oC to ensure the homogenous mixing to form a stable suspension B. A and B were mixed together stirred for several minutes and transferred

into a 500 mL reaction vessel placed in a conventional microwave oven. The solution is then irradiated with microwave for 5 sec. on and off for 300 sec., and cooled at room temperature filtered with whatman filter paper. The resultant powder was washed 3 times with distilled water and transferred into a dry oven for 6 h at 90 °C. The powder was then heat treated at 500 °C for 1 h in electric furnace. The weight ratios of GO to $CoSe_2$ and TiO_2 were taken as 0.5 %, 1.5% and 2.5% the obtained samples were labeled as CGT1, CGT2, CGT3 respectively.

2.5. Photocatalytic hydrogen evolution system

The photocatalytic reaction was carried out at room temperature. The photocatalyst powder, 50 mg $CoSe_2$/graphene/TiO_2, was dispersed by a magnetic stirrer in 200 ml aqueous solution containing 0.06 mol L^{-1} Na_2S, 0.04 mole L^{-1} Na_2SO_3 and 20% methanol as a sacrificial reagent. A 356-nm UV light source was employed at a distance of 20 cm from the glass reactor. The amount of hydrogen gas evolved was detected by a Minimax (X13010683) XP H_2 sensor.

2.6. Characterization

To determine the crystal phase and the composition of the as-prepared $CoSe_2$/graphene-TiO_2 samples, XRD characterization was carried out at room temperature using XRD (Shimata XD-D1, Japan) with Cu Kα radiation (λ=1.54056 Å) in the range of 2θ = 10-80^o at a scan speed of 1.2^o m^{-1}. Transmission electron microscopy (TEM, JEOL, JEM-2010, Japan) was used to observe the surface state and structure of the photocatalyst composites at an acceleration voltage of 200 kV. TEM was also used to examine the size and distribution of the $CoSe_2$ particles deposited on the graphene sheet. Diffuse reflectance spectra were obtained using a scan UV-vis spectrophotometer (Neosys-2000) equipped with an integrating sphere assembly. Scanning electron microscope SEM (JSM-5200 JOEL, Japan) was used to observe the surface state and morphology of the prepared nanocomposites. The morphology of the samples was studied using energy dispersive X-ray spectroscopy (EDX), which was also employed for elemental analysis. Transmission electron microscopy (TEM, JEOL, JEM-2010, Japan) was used to observe the surface state and structure of the photocatalyst composites at an acceleration voltage of 200 kV. X-ray photoelectron spectroscopy (XPS) was performed using VG scientific VISACA lab 2000 and a monochromatic Mg X-ray radiation source. Diffuse reflectance spectra were obtained using a scanning UV/Vis spectrophotometer (Neosys-2000) equipped with an integrating sphere assembly. Raman spectra of the samples were observed using a spectrometer (Jasco Model Name NRS-3100) with an excitation laser wavelength of 532.06 nm.

3. Results and Discussions

3.1. Growth and Characterization of $CoSe_2$/graphene-TiO_2 Nanocomposites

The synthesis method for our nanocomposites is shown in Scheme 1. As it is already known that microwave radiation need a polar solvent for synthesis of nanomaterials. We consider ethylene glycol as a solvent in our experiments. These polar solvents absorb microwave energy and limit localized heating and causes decomposition The advantage of microwave synthesis are, i.e., short reaction time, saving of long usage of power, extra cooled water for reflux and closed vessel to release minimum toxic gases to environment [17-19]. The high energy microwave generates hot spot, with extremely high localized temperature and pressure which tends to accelerate the nanoparticles and simultaneous attachment occur on graphene sheet [20-21].

The identification of the crystal phases was analyzed through XRD techniques as depicted in Fig. (1). The bare TiO_2 and $CoSe_2$-G have a diffraction pattern that corresponds to the cubic cobalt selenide structure which confirms the formation of cubic crystalline structure on graphene sheet [22]. Fig. 1 depicts the XRD pattern of the $CoSe_2$-G nanocomposites. The diffraction peak of $CoSe_2$ (111) and graphene (002) are located at 26° at 2θ. It is difficult to distinguish both peaks as a result of the broad reflection from the $CoSe_2$. The $CoSe_2$-G composites with different compositions exhibit the characteristic (111), (200), (210), (211), (220), and (311) (230), (321), (400), (421), (511), reflections that correspond to the crystal phase (JCPDS PDF#: 00-065-3327). The TiO_2 diffraction peak (101) and graphene 002) peaks are located at the same 2θ values. The nanocomposites contain characteristic reflections (101), (004), (200), (105), (211), and (220) that correspond to the anatase crystal phase (JCPDS PDF#: 00-021-1272). The Fig. 1, shows a slight decrease in intensity of the CGT1 nanocomposites as compare to TiO_2 and $CoSe_2$-G. The distortion is not completely related with the decrease in intensity. But in light of reported results we assume that the suppression of peaks leads towards distortion of crystalline phase of semiconductor materials on graphene sheet [23-24]. The interaction of nanoparticle with graphene surface creates a phonon confinement effect by decreasing the probability of spherical shape nanoparticles. Therefore we observed some tube type TiO_2 nanoparticle in the composite as depicted in TEM images of ternary composites.

We examined the morphological structure of our nanocomposites by scanning electron microscopy as shown in Fig. 2. The $CoSe_2$-graphene nanocomposites depict the plate like morphology of graphene while the particle size and shape is difficult to visualize in SEM. The

SEM image was taken to describe the overall morphology and shape of graphene in the composite. From this figure the overall structure can be clearly predicted that graphene is sheet like structure broken off in different direction. Both images in Fig 2(a-b), shows $CoSe_2$ may be spherical shape with partial agglomeration. After microwave treatment, the sheet morphology is retained and the graphene surfaces are covered with $CoSe_2$ nanoparticles. The anchoring of nanoparticle is very helpful to overcome the interactions between the functionalities on graphene surface. Fig. 3(a-c) assigns to the $CoSe_2$/graphen-TiO_2 nanocomposites. From these images we can clearly observe the difference between binary and ternary composites. After attachment of TiO_2 the brighter spot arises in the ternary composite. We assumed that TiO_2 also reside on graphene surface supporting $CoSe_2$ nanoparticles. Further TEM images confirm the shape of these TiO_2 and $CoSe_2$ nanoparticles.

TEM analysis was carried out to further study the microscopic structural information of binary $CoSe_2$/graphene composites as shown in Fig. 4(a-b). The images in Fig. 4(a-b) were taken with the same magnification so that the large surface structure and the overall history of the nanoparticles and graphene sheet were exposed. This image shows that the graphene sheets are well distributed, providing a large micro sheet type plate structure for the $CoSe_2$ nanoparticles. The overall image indicates that significantly less agglomeration of the nanoparticles on the graphene sheet is observed. Fig. 4(b) further confirms that almost spherical nanoparticles with uniform sizes are observed on graphene sheet.

Fig. 5, shows TEM image of the CGT2 nanocomposites. TEM analysis was carried out to further study the microscopic structural information of ternary CoSe2/graphene-TiO_2 nanocomposites as shown in Fig. 5 (a-d). The images in Fig. 5(a-b) demonstrate the 100 and 50 nm magnification images of the CGT2 nanocomposites. From these images tube type TiO_2 can be seen with partial agglomeration. We assume that the seeming agglomeration is due to large size of the TiO_2 nanotube having length more than 100 nm. To further investigate the shape and size of nanocomposites we performed the high resolution TEM images with 20 and 5 nm as shown in Fig. 5(c-d). As it can be seen from the high magnification images that TiO_2 nanotubes were found supporting $CoSe_2$ nanoparticles on graphene sheet. Thus, we can say that microwave assisted synthesis of $CoSe_2$/graphene-TiO_2 is advantageous over other synthesis methods, and would be beneficial for the improved photocatalytic property of these materials.

The Raman spectra of $CoSe_2$/graphene-TiO_2 nanocomposites shows two prominent peaks corresponds to D band and G band as depicted in Fig. (6). The D band is induced by defects, while the G band is induced by sp^2 carbon bonds. Fig. 6, depicted the micro Raman spectra of our nanocomposites with G band and D band correspond to the vibration of carbon atom in disorder or defects site and in plane vibration of sp^2 bonded carbon atoms respectively [16]. The difference in the Raman band intensity or shift provides information about the nature of the defects and C-C bonds [25-26]. The peaks observed below 600 cm^{-1} in Fig. 6 (a) are attributed to $CoSe_2$ crystal. The peaks around 200cm^{-1} to 300cm^{-1} wave number are attribute to some Se^o trigonal phase. And the peaks around 410cm^{-1} and 510 cm^{-1} seems to be associated with the cubic $CoSe_2$ phase. The $CoSe_2$/graphene-TiO_2 nanocomposite in Fig. 6 (b-d) shows slight different Raman spectra as compared to $CoSe_2$-G.

The order of defects in the graphene or graphene oxide can be reflected by the intensity ratio of the D to the G band. The calculate I_D/I_G of the $CoSe_2$/graphene nanocomposites were found to be ~ 0.981, while for CGTs ternary nanocomposites this value were found to be 1.006. These empirical results depicts that the introduction of TiO_2 still affect the ratio and increase amount of defects were found. Another important observation is the shift of G peaks towards higher frequency compared to binary $CoSe_2$/graphene nanocomposites. The observed shift was found to be ~20cm^{-1}. There are several possible origins for the shift of Raman peaks; these may be inclusion of semiconductors i.e., $CoSe_2$ and TiO_2 as dopant, the laser excitation during Raman experiment, and the electron/hole created during this excitation by the attached semiconductor materials [27-29]. There are some characteristic peaks observed located at 148, 390, 516, and 640 cm^{-1} correspond to the Eg(1), B1 g(1), A1g + B1 g(2), and Eg(2) modes of anatase TiO_2 [30-31].

A comparison of the absorption spectra of $CoSe_2$/graphene-TiO_2 nanocomposites is displayed in Fig. 7(a-e). There is an enhanced absorbance towards the visible region >500 nm was observed with ternary compounds. Meanwhile the graphene based $CoSe_2$ gives the absorbance smaller than ternary composites. This enhanced absorbance may be attributed to the optimum loading of the support material on graphene and the homogeneous distribution of nanoparticles by providing large number of reaction cites. From the figure we can see that bare TiO_2 has sharp edge in the UV region which has been improved by introducing it in ternary graphene based materials. The unpaired π electron in graphene may cause the interaction with metal or

semiconductors nanoparticles, such interaction might shift the band edge and will increase the light absorption towards the visible region [32]. Lee et al also observed such kind of effect with titanium nanoparticles and observed the optical response towards the visible region of electromagnetic spectrum [33].

The estimation of the band gap was carried out using Kubelka Mulk transformation by converting the reflectance plot according to Tauc condition. The following equation was proposed by Tauc, Davis, and Mott.

$$(h\nu\alpha)^{1/n} = A(h\nu - E_g) \quad (1)$$

Where h is plank constant, ν is frequency of vibration, α is the absorption coefficient, E_g is band gap and A proportional constant. In this calculation the vertical axis is converted to quantity called F(R∞), which is proportional to the absorption coefficient. Thus the α in the Tauc plot in equation is substituted with the function F(R∞). The actual relational expression becomes

$$(h\nu\ F(R\infty))^2 = A(h\nu - E_g) \quad (2)$$

using the KM function, the $(h\nu\ F(R\infty))^2$ was plotted against the hν. The curve having $(h\nu\ F(R\infty))^2$ on the horizontal and hν on the vertical axis defines the precise band gap our nanocomposites. A line drawn tangent to a point of inflection on the curve and the hν value at that point defines the estimated band gap of the nanocomposites. The obtained plots are given in Fig. (8).

The band gap energies were found to be in order of TiO_2 (inset Fig. 8) > $CoSe_2$-G > CGT1> CGT3> CGT2 of the $CoSe_2$/graphene-TiO_2 nanocomposites. The differences in the band gap of our nanocomposites may possibly attribute to the distribution of $CoSe_2$ particles and TiO_2 nanotubes on the graphene sheet. Similarly the partial agglomeration can also affect the absorption property and hence may result in band gap variation. Another reason for the variation of the band gap may be the different amounts of graphene in the composites, which considerably affects the optical property of our ternary nanocomposites. Therefore, reduction in the band gap is observed for the nanocomposites [34-35]. Further enhanced visible light absorption occurred on the ternary $CoSe_2$/graphene-TiO_2 photocatalyst confirming effectively enhanced light-harvesting activity due to the synergetic effect of $CoSe_2$ and graphene as co-modifiers.

3.2. Photocatalytic hydrogen production studies:

The role of ternary graphene based materials in improving catalytic activity was studied by monitoring the photocatalytic hydrogen production from aqueous solution containing

Na_2S/Na_2So_3 and methanol as sacrificial reagent. The CGT2 composites of ternary $CoSe_2$/graphene-TiO_2 composite gives hydrogen evolution rate of 205 μmol h^{-1} which is greater than all other samples in the composites as depicted in Fig. (9). Furthermore the P25 and $CoSe_2$/graphene nanosheets give a smaller value of hydrogen evolution rate than ternary system. The value of hydrogen evolution rate for this bare (P25) and binary system is almost 6 times and 1.5 times lesser than the ternary system. The comparison clearly shows that graphene based ternary system greatly improve the catalytic property indicating a strong interaction between graphene and attached semiconductor materials. It is no doubt that the spherical $CoSe_2$ supported by tube type TiO_2 allows a good interfacial contact with graphene sheet by boosting the synergistic effect between $CoSe_2$ and graphene sheet. Similarly the dependence of different amount of graphene also plays a crucial role in catalytic hydrogen evolution. The optimal content of graphene in the $CoSe_2$/graphene-TiO_2 system is determined to be 1.5 wt%. The higher content may leads towards smaller rate probably due to increased light absorption of graphene itself which disparately harms the excitation of $CoSe_2$ and TiO_2 in the composites.

As compared to our previous report, the photocatalytic H_2 evolution for Pt/graphene nanocomposites and P-25 were found to be marginally smaller than the present nanocomposites with TiO_2 [36]. The graphene, as an electron acceptor/transporter, can promote the separation of the photo generated electron-hole pairs in the ternary system; efficiently transport the photo generated electrons to TiO_2 valance band by creating a donor level to transfer to conduction band and finally improving the photocatalytic H_2 production. The role of the sacrificial reagent is to provide electrons to consume the photo generated holes to further increase the catalytic properties, which will help to increase the recombination time in our nanocomposites [37].

The hydrogen evolution plot for the 20% methanol solution is shown in Fig. (10). A relatively lower amount of hydrogen evolution rate (190 μmol) was reported compared to Na_2S/Na_2SO_3 aqueous solution. The work function of graphene is higher than that of the reagent at the interface between $CoSe_2$ and graphene. This means that the electron transfer from graphene was energetically favorable. Due to the high electron affinity of graphene resulting from the giant π-π conjugated structure, the electron transfer from $CoSe_2$ to graphene continues until the two systems attain charge equilibrium [38-39].

The shaped double charge layers stabilize the accepted electrons and gather in the graphene network. This decelerates the continuous addition of electrons from the reagents to the graphene

sheet. If the trapped electrons are not transferred well, they are forced to be transferred back to recombine with the electron donors, which would lower the catalytic efficiency. In case of methanol solution the lower catalytic hydrogen may due to the recombination of donor electron in the catalytic process [40-41]. In case of methanol solution the CGT2 composite shows improved photocatalytic hydrogen evolution rate than other nanocomposites.

To address the stability of photocatalyst containing sulfides as a sacrificial reagent is very important because of the well-known process of photocorosion of sulfides. A time circle experiment was carried out to estimate the stability of our ternary $CoSe_2$/graphene-TiO_2 system. The respective hydrogen evolution rate was found for the CGT2 nanocomposite in the range of 198 to 195.5 $\mu molh^{-1}$, after 5 cyclic tests as shown in Fig. (11). There is no obvious change in the activity of the composites after 5 cycles. This suggests that $CoSe_2$/graphene-TiO_2 have an excellent stability and can be used for continuous photocatalytic hydrogen evolution system. This great improvement and stability of our ternary graphene system can be understood as follows; an effective charge carrier system at the interface of graphene and $CoSe_2$ which is provided by graphene itself, the synergistic effect between $CoSe_2$ and graphene, the excellent charge transfer ability of graphene can accept electrons form conduction band of $CoSe_2$ and transfer it to TiO_2 via graphene sheet. These electrons through the conduction band of TiO_2 reduce water to H_2 while the holes in $CoSe_2$ oxidize water to O_2, achieving a complete water splitting cycle through our designed photocatalyst material as shown in Fig. (12). Similarly the sheet morphology of graphene can reduce the diffusion length of photoexcited electron and holes form the bulk to the surface for resultant oxidation and reduction reaction.

Conclusion:

In summary the heterogeneous $CoSe_2$/graphene-TiO_2 were synthesized through a fast microwave assisted technique. TEM images clearly indicate that the tube types TiO_2 are distributed on surface of graphene sheet supported by $CoSe_2$ nanoparticles. As results of heterostructure the promotion of the excited charge carriers at the interface of $CoSe_2$ and graphene was found to be highest due to synergistic effect of graphene and $CoSe_2$ by increasing the recombination time. The graphene in the system act as solid state electron mediator to support the ternary system and will help to provide stable photocatalyst heterogeneous materials. The optical properties were also observed to be affected by the different weight% of graphene in the composites by

observing their respective band gaps from DRS spectra. The present study has cemented a new way of using graphene based materials for developing efficient heterosystem for hydrogen production.

Acknowledgement: This work was supported by research foundation of Hanseo University in the year 2014. The authors are grateful to the University for financial support.

References:

[1] K. Maeda, M. Higashi, D. L. Lu, R. Abe and K. Domen, Efficient nonsacrificial water splitting through two-step photoexcitation by visible light using a modified oxynitride as a hydrogen evolution photocatalyst. J. Am. Chem. Soc., 2010, 132, 5858–5868.

[2] K. Sayama, K. Mukasa, R. Abe, Y. Abe and H. Arakawa, Stoichiometric water splitting into H2 and O2 using a mixture of two different photocatalysts and an IO3-/I- shuttle redox mediator under visible light irradiation. Chem. Commun., 2001, 2416–2417.

[3] K. Sayama, K. Mukasa, R. Abe, Y. Abe and H. Arakawa, A new photocatalytic water splitting system under visible light irradiation mimicking a Z-scheme mechanism in photosynthesis J. Photochemical. Photobiol., A, 2002, 148, 71–77.

[4] S. Hara and H. Irie, Band structure controls of $SrTiO_3$ towards two-step overall water splitting, Appl. Catal., B, 2012, 115, 330–335.

[5] S. Hara, M. Yoshimizu, S. Tanigawa, L. Ni, B. Ohtani and H. Irie, Hydrogen and oxygen evolution photocatalysts synthesized from strontium titanate by controlled doping and their performance in two-step overall water splitting under visible light J. Phys. Chem. C, 2012, 116, 17458–17463.

[6] H. Tada, T. Mitsui, T. Kiyonaga, T. Akita and K. Tanaka, All-solid-state Z-scheme in CdS-Au-TiO_2 three-component nano junction system Nat. Mater., 2006, 5, 782–786.

[7] H. J. Yun, H. Lee, N. D. Kim, D. M. Lee, S. Yu and J. Yi, A combination of two visible-light responsive photocatalysts for achieving the Z-scheme in the solid State, ACS Nano, 2011, 5, 4084–4090.

[8] C. Chen, W. Cai, M. Long, B. Zhou, Y. Wu, D. Wu, Y. Feng, Synthesis of visible-light responsive graphene oxide/TiO_2 composites with p/n heterojunction. ACS Nano 2010, 4, 6425−6432.

[9] J. S. Lee, K. H. You, C. B. Park, Highly photoactive, low bandgap TiO_2 Nanoparticles wrapped by graphene. Adv. Mater. 2012, 24, 1084−1088.

[10] P. Chen, T. Y. Xiao, Y. H. Qian, S. S. Li and S. H. Yu, A nitrogen-doped graphene/carbon nanotube nanocomposite with synergistically enhanced electrochemical activity. Adv. Mater., 2013, 25(23), 3192-3196.

[11] H. Zhang, X. Lv, Y. Li, Y. Wang and J. Li, P25-graphene composite as a high performance photocatalyst. ACS Nano, 2010, 4, 380-386.

[12] Q. J. Xiang, J. G. Yu and M. Jaroniec, Graphene-based semiconductor photocatalysts, Chem. Soc. Rev., 2012, 41, 782-796.

[13] N. Zhang, Y. Zhang, X. Pan, M. Q. Yang and Y.-J. Xu, Constructing Ternary CdS–Graphene–TiO2 hybrids on the flatland of graphene Oxide with enhanced visible-light photoactivity for selective transformation, J. Phys. Chem. C, 2012, 116, 18023–18031.

[14] K. Ullah, Z. D. Meng, S. Ye, L. Zhu and W. C. Oh, Synthesis and Characterization of Novel PbS-Graphene/TiO_2 composite with enhanced photocatalytic activity, J. Ind. Eng. Chem., 2014, 20(3), 1035–1042.

[15] N. Zhang, S. Liu and Y.-J Xu, Recent progress on metal core@semiconductor shell nanocomposites as a promising type of photocatalyst, Nanoscale, 2012, 4, 2227–2238.

[16] Kefayat Ullah, Shu Ye, Sun-Bok Jo, Lei Zhu, Kwang-Youn Cho, Won-Chun Oh, Optical and photocatalytic properties of novel heterogeneous $PtSe_2$–graphene/TiO_2 nanocomposites synthesized via ultrasonic assisted techniques, Ultrasonics Sonochemistry, 21 (2014) 1849–1857

[17] E.-P. Ng, D. T.-L. Ng, H. Awala, K.-L. Wong and S. Mintova, Microwave synthesis of colloidal stable AlPO-5 nanocrystals with high water adsorption capacity and unique morphology, Mater. Lett., 2014, 132, 126–129.

[18] L. Zhang, X. Chen, S. Jin, J. Guan, C. T. Williams, Z. Peng and C. Liang, Rapid microwaves synthesis of CoSix/CNTs as novel catalytic materials for hydrogenation of phthalic anhydride, J. Solid State Chem., 2014, 217, 105–112.

[19] K. Ullah, S. Ye, Z. Lei, K.Y. Cho and W. C. Oh, Synergistic effect of $PtSe_2$ and graphene sheets supported by TiO_2 as cocatalysts synthesized via microwave techniques for improved photocatalytic activity, Catal. Sci. Technol., 2015, 5, 184-198

[20] Gu L., L. Qian, Y. Lei, Y. Wang, J. Li, H. Yuan and D. Xiao, Microwave-assisted synthesis of nano sphere-like NiCo2O4 consisting of porous nanosheets and its application in electro-catalytic oxidation of methanol, J. Power Sources, 2014, 261, 317–323.

[21] K. Ullah, S. Ye, L. Zhu, Z. D. Meng, S. Sarkar and W. C. Oh, Microwave assisted synthesis of a noble metal-graphene hybrid photocatalyst for high efficient decomposition of organic dyes under visible light, Mater. Sci. Eng., B, 2014, 180, 20–26.

[22] S. D. Perera, R. G. Mariano, K. Vu, N. Nour, O. Seitz, Y. Chabal and K. J. Balkus Jr., Hydrothermal synthesis of graphene-TiO2 nanotube composites with enhanced photocatalytic activity, ACS Catal., 2012, 2, 949–956.

[23] Biljana Pejova, Optical phonons in nanostructured thin films composed by zinc blende zinc selenide quantum dots in strong size-quantization regime: Competition between phonon confinement and strain-related effects, J. Solid State Chem., 2014, 213, 22–31.

[24] B. D. Cullity, Elements of X-rays Diffraction, Addison Wesley Publishing Co, Philippines, 2nd edn, 1978, ch. 10, p. 338.

[25] E. Anastassakis, light scattering in transition metal diselenide $CoSe_2$ and $CuSe_2$, Solid State Communications, Vol. 13, 1973, pp. 1297-1301.

[26] L. Zhu, M. Teo, P.C. Wong, K.C. Wong, I. Narita, F. Ernst, K.A.R. Mitchell, S.A. Campbell, Synthesis, characterization of a $CoSe_2$ catalyst for the oxygen reduction reaction, Applied Catalysis A: General 386 (2010) 157–165

[27] Das A, Pisana S, Chakraborty B, Piscanec S, Saha SK, Waghmare UV, et al. Monitoring dopants by Raman scattering in an electrochemically top-gated graphene transistor. Nat anotechnol, 3, 2008, 210–215.

[28] Ni ZH, Yu T, Luo ZQ, Wang YY, Liu L, Wong CP, et al. Probing charged impurities in suspended graphene using Raman spectroscopy. ACS Nano 2009, 3 (3), 569–574.

[29] Ni ZH, Yu T, Lu YH, Wang YY, Feng YP, Shen ZX. Uniaxial strain on graphene: Raman spectroscopy study and bandgap opening. ACS Nano, 2 (11), 2008, 2301–2305.

[30] Q. J. Xiang, J. G. Yu and M. Jaroniec**,** Enhanced photocatalytic H_2-production activity of graphene-modified titania nanosheets, Nanoscale, 2011, 3, 3670-3678.

[31] G. M. Zhou, D. W. Wang, L. C. Yin, N. Li, F. Li and H. M. Cheng, Oxygen Bridges between NiO Nanosheets and Graphene for Improvement of Lithium Storage, ACS Nano, 2012, 6, 3214-3223

[32] D. Kong, H. Wang, Z. Lu, and Yi Cui, $CoSe_2$ Nanoparticles grown on carbon fiber paper: An efficient and stable electrocatalyst for hydrogen evolution Reaction, J. Am. Chem. Soc., 2014, 136 (13), pp 4897–4900

[33] Lee, J. S. You, K. H. Park, C. B. Highly photoactive, low bandgap TiO_2 nanoparticles wrapped by graphene, Adv. Mater. 2012, 24, 1084−1088.

[34] R. Rao, R. Podila, R. Tsuchikawa, J. Katoch, D. Tishler, A. Rao, I M. shigami, Effects of Layer Stacking on the Combination Raman Modes in Graphene, ACS Nano , 2011, 5 (3), 1594–1599.

[35] K. John, D.T. Manolis, D.P. George, N.A. Mariza, S.T. Kostas, G. Sofia, B. Kyriakos, K. Christos, O. Michael, L. Alexis, Highly active catalysts for the photo oxidation of organic compounds by deposition of fullerene onto the MCM-41 surface: A green approach for the synthesis of fine chemicals, Applied Catalysis B: Environmental, 117–118 (2012), pp. 36–48.

[36] K. Ullah, S. Ye, L. Zhu, S. B. Jo, W. K. Jang, W. C. Oh, Noble metal doped graphene nanocomposites and its study of photocatalytic hydrogen evolution Solid State Sciences, 31, 2014, 91-98.

[37] Guancai Xie, Kai Zhang, Beidou Guo, Qian Liu, Liang Fang, and Jian Ru Gong, Graphene-based materials for hydrogen generation from light-driven water splitting, Adv. Mater. 2013, 25, 3820–3839

[38] Kamat PV. Graphene-based nano architectures: Anchoring semiconductor and metal nanoparticles on a two dimensional carbon support J Phys Chem Lett 2010; 1, 520-527.

[39] P. Hu, Y. D. Posner, Y. B. David, and D. Milstein, Reusable homogeneous catalytic system for hydrogen production from methanol and water, ACS Catal., 2014, 4 (8), 2649–2652

[40] B. J. Ma, J. S. Kim, C. H. Choi, S. I. Woo, Enhanced hydrogen generation from methanol aqueous solutions over $Pt/MoO_3/TiO_2$ under ultraviolet light, international journal of hydrogen energy, 38, (2013) 3582-3587

[41] K. Ullah, A. Ali, S. Ye, L. Zhu, W. C. Oh, Microwave-Assisted Synthesis of Pt-Graphene/TiO_2 nanocomposites and their efficiency in assisting hydrogen evolution from water in the presence of sacrificial agents, Science of Advanced Materials, 04/2015, 7(4), 606-614.

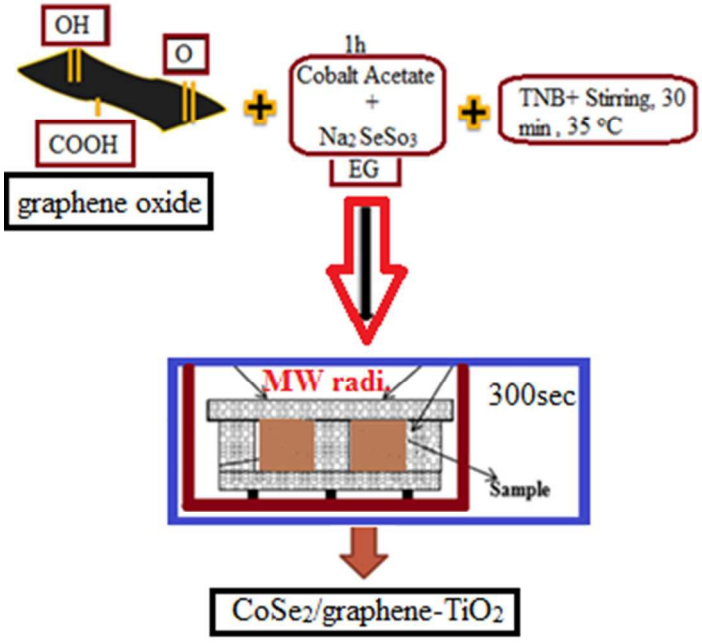

Scheme1. Fabrication method for $CoSe_2$-graphene/TiO_2 nanocomposites

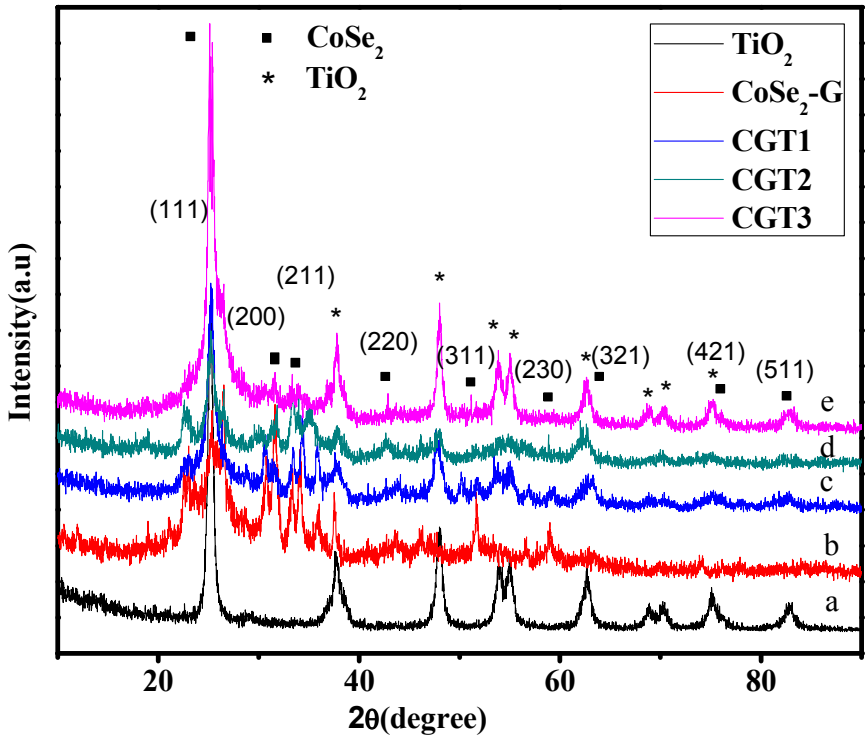

Fig. 1. (a-e); XRD pattern of $CoSe_2$/graphene-TiO_2 nanocomposites ;(a) TiO_2 (b) $CoSe_2$-G (c) CGT1 (d) CGT2 (e) CGT3

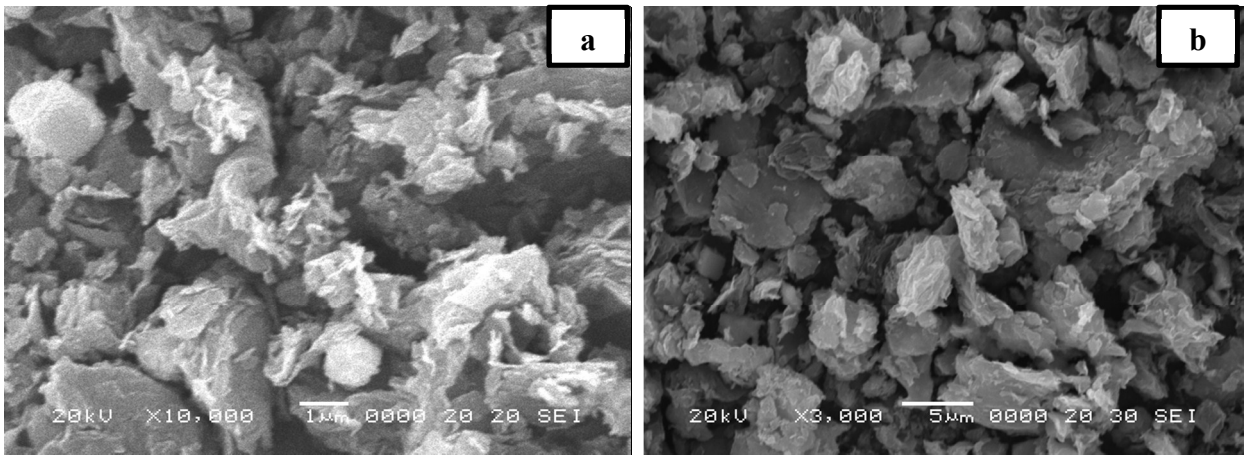

Fig. 2. SEM micrograph of $CoSe_2$-G nanocomposite.

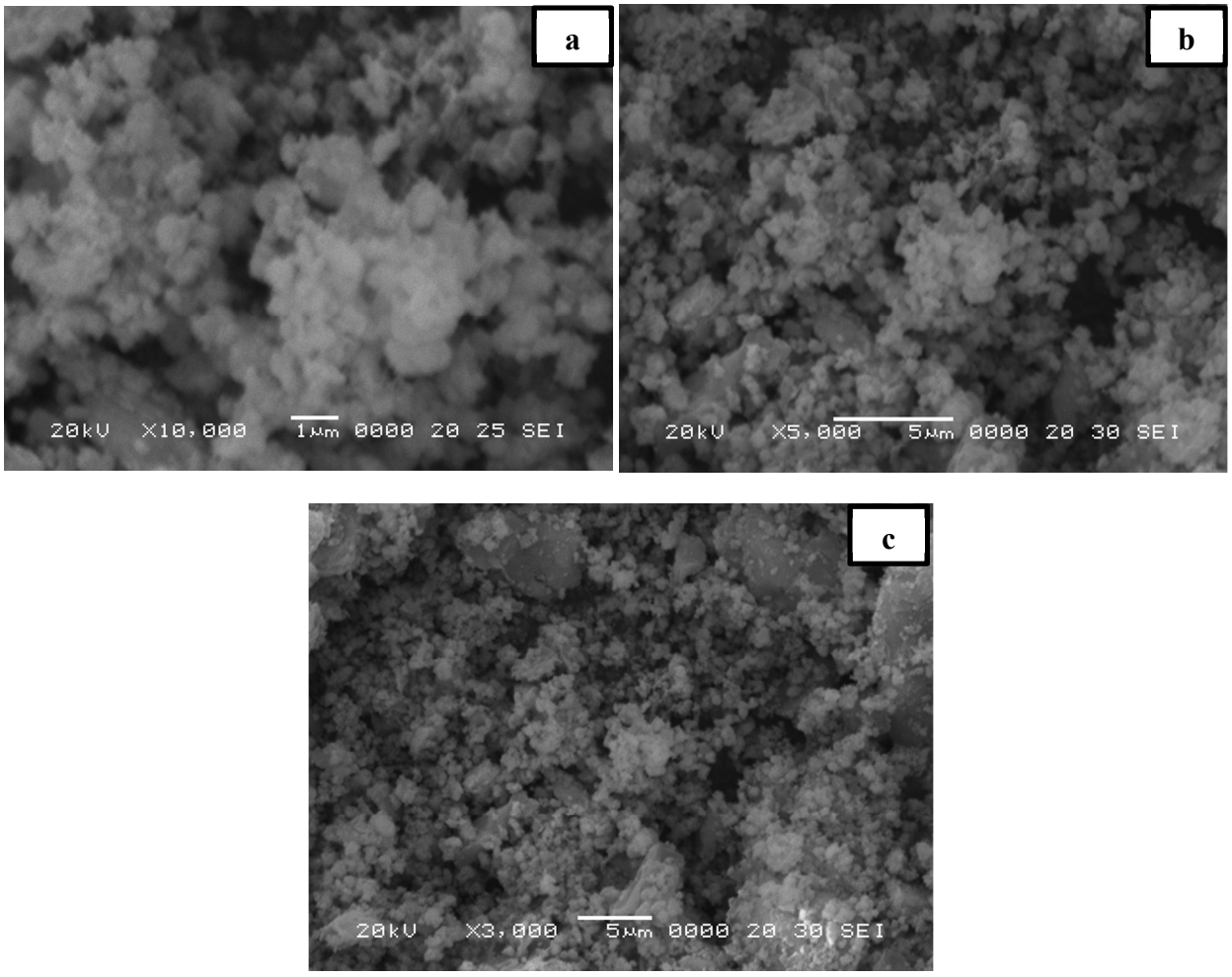

Fig. 3. SEM images of CGT2 nanocomopsites

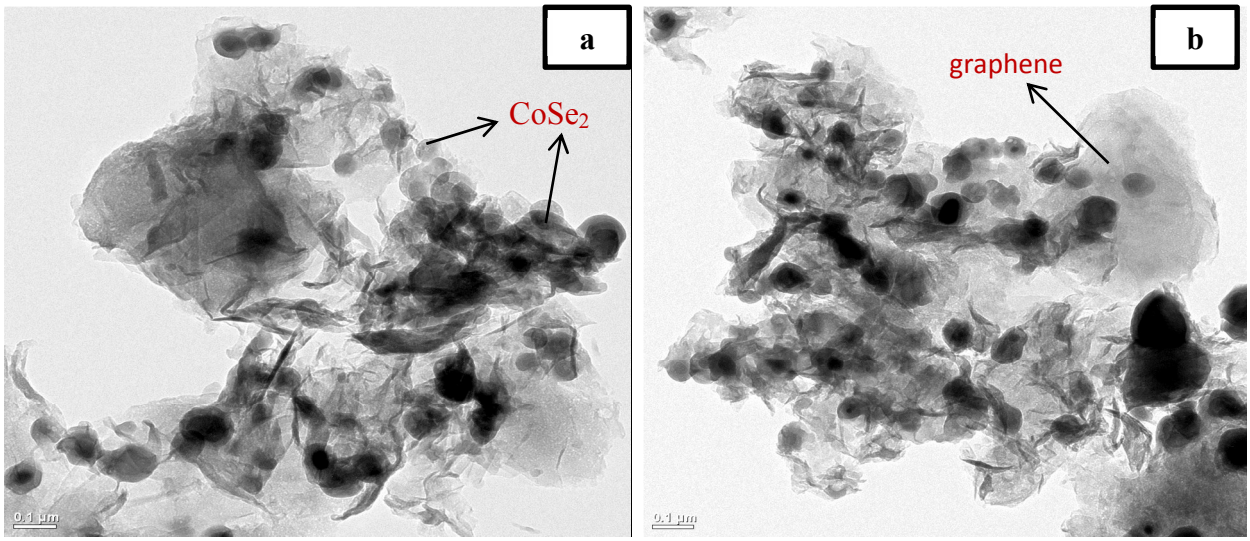

Fig. 4(a-b). TEM images showing $CoSe_2$-G nanocomposites

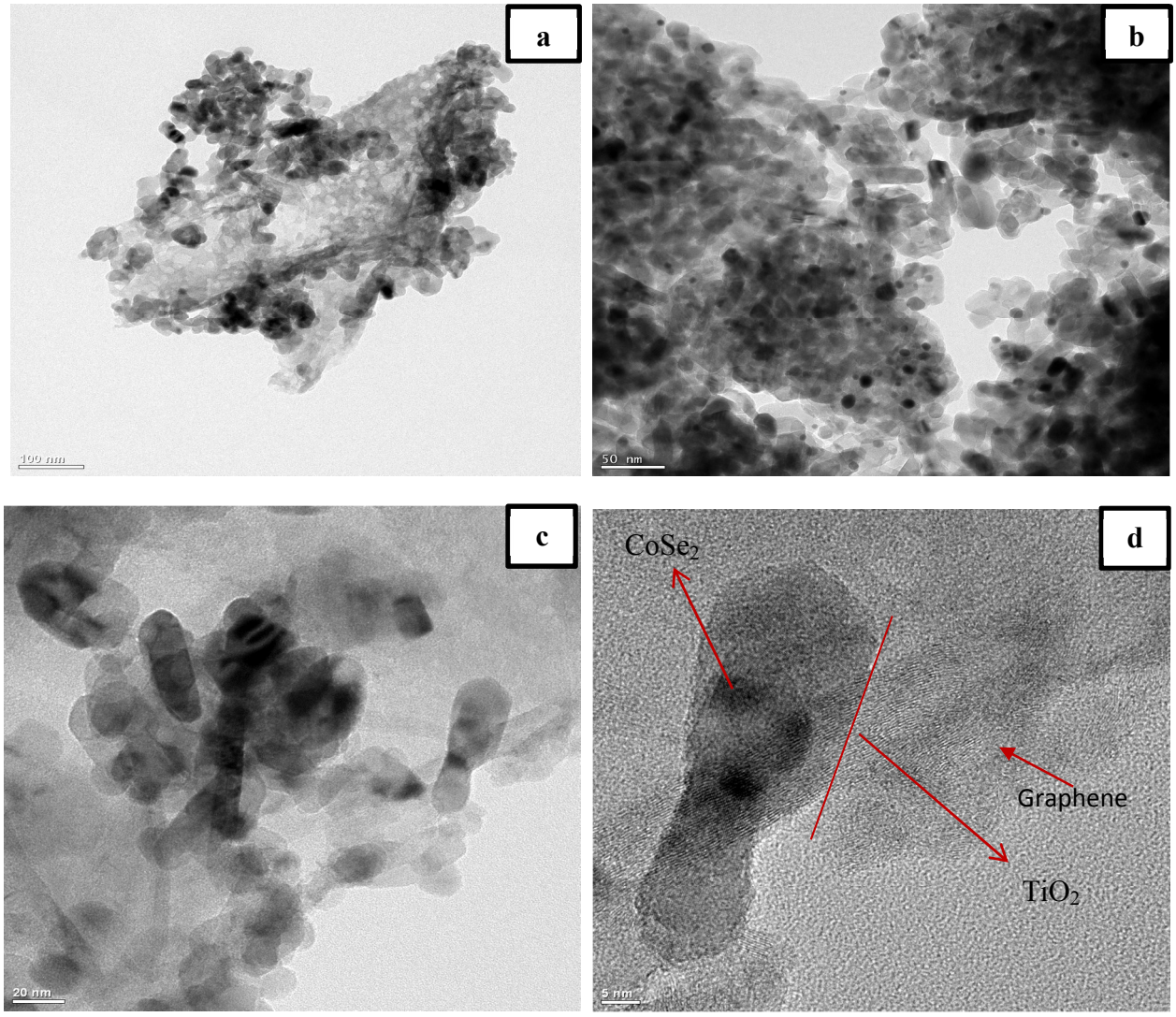

Fig. 5(a-d). TEM Images of CGT2 nanocomposites;(a) 100nm (b) 50nm (c) 20nm (d) 5nm

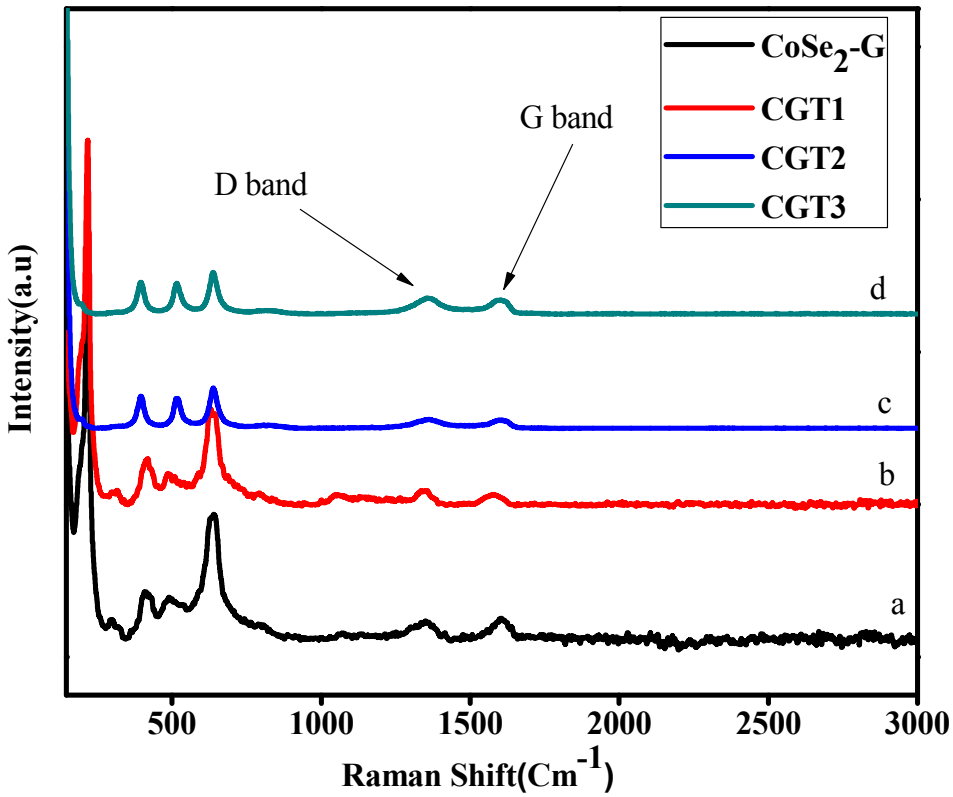

Fig. 6. Raman spectra of (a) $CoSe_2$-G (b) CGT1 (c) CGT2 (d) CGT3

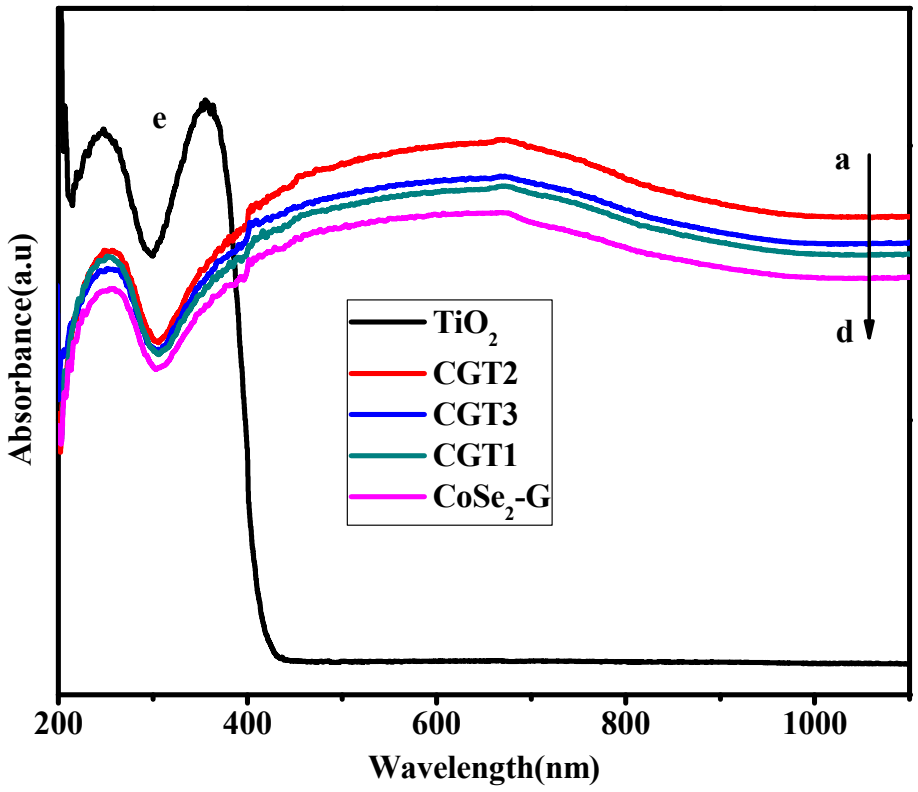

Fig. 7. DRS spectra of (a) $CoSe_2$-G (b) CGT1 (c) CGT3 (d) CGT2 (e) TiO_2

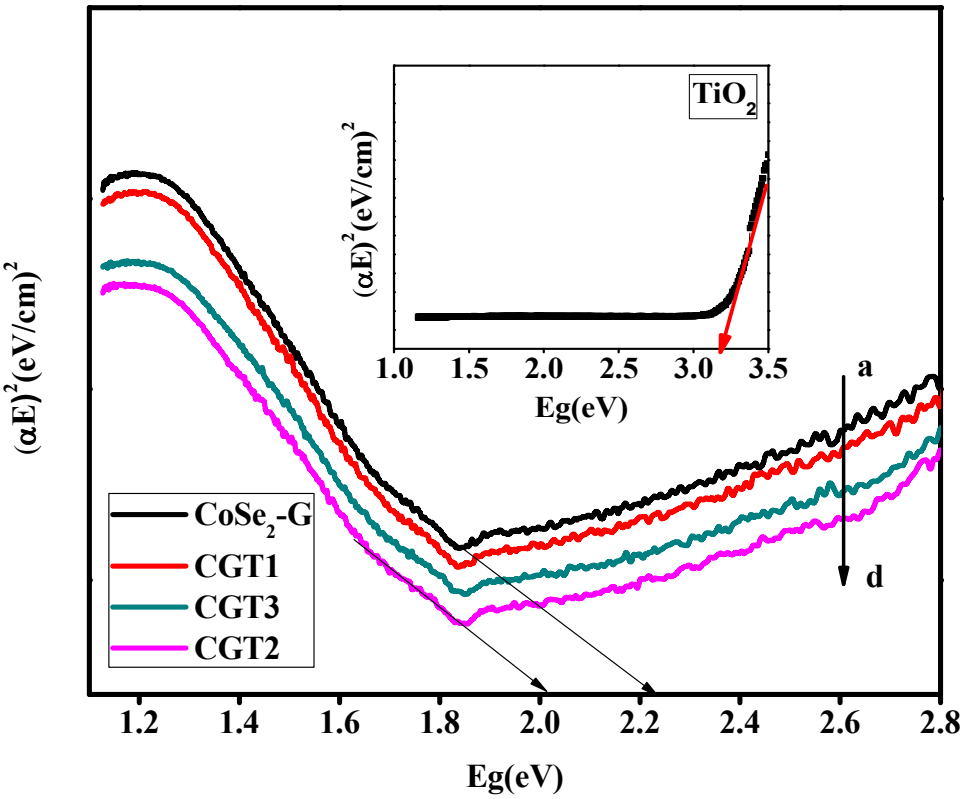

Fig. 8. Transform Kubelka Munk function verses photon energy; (a) $CoSe_2$-G (b) CGT1 (c) CGT3 (d) CGT2 Inset . (e) TiO_2

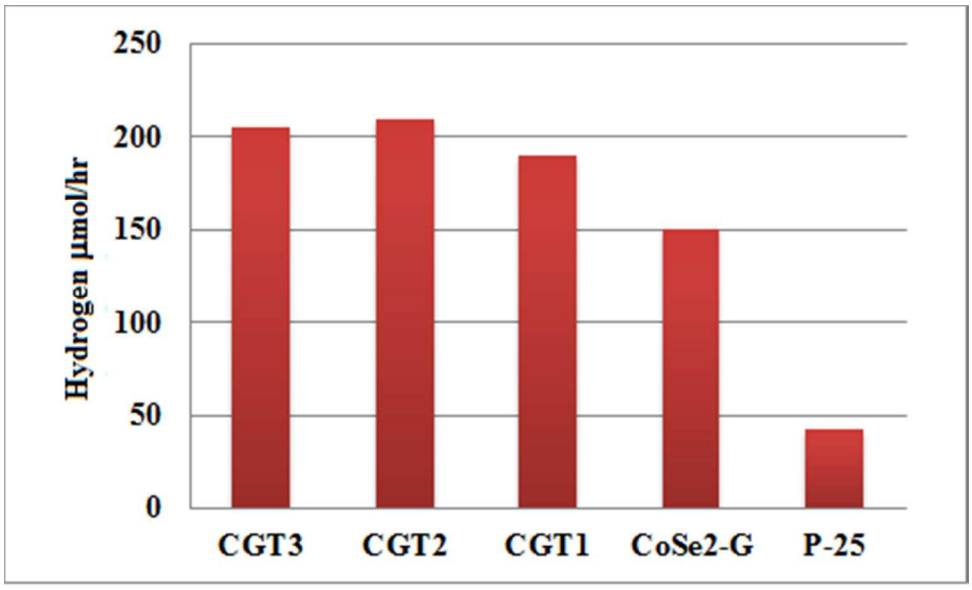

Fig. 9. Reaction time profile of H_2 evolution under UV light illumination from aqueous solution containing Na_2S/Na_2SO_3 with CGT(1-3) composites, $CoSe_2$-G and P-25 as photocatalyst

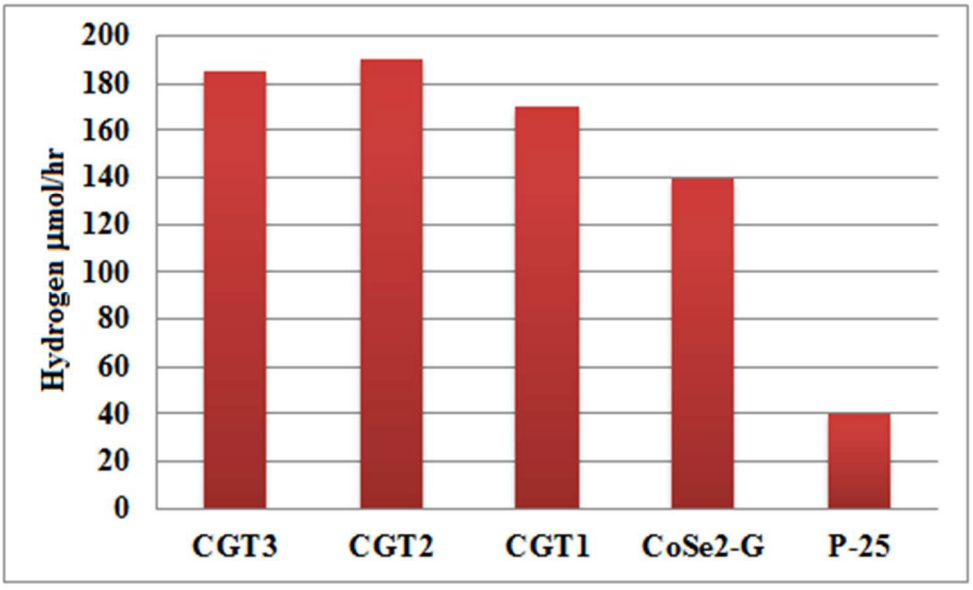

Fig. 10. Hydrogen production rate from an aqueous solution containing 25 % methanol with CGT (1-3) composites, $CoSe_2$-G and P-25 as photocatalyst

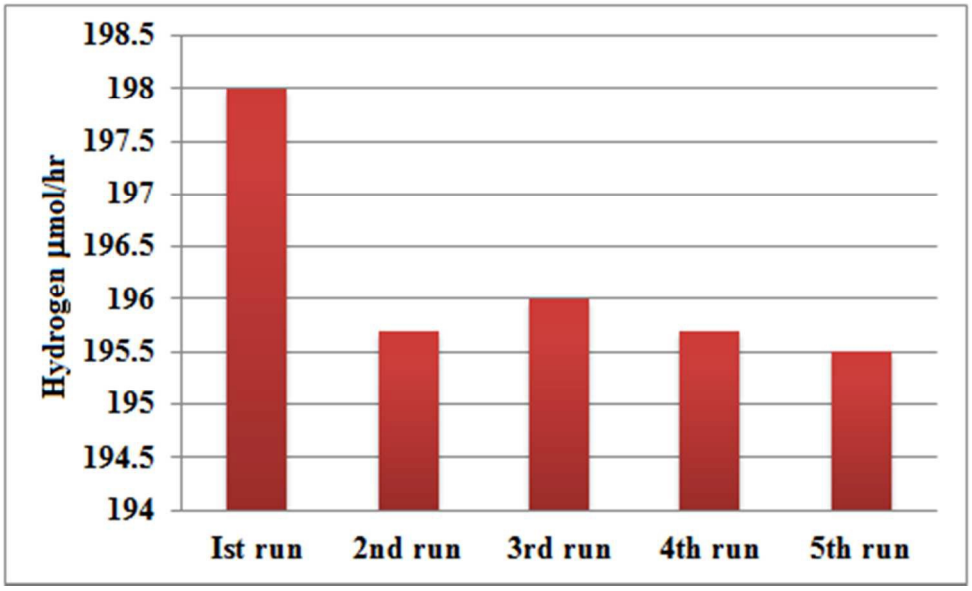

Fig. 11. Cyclic test for CGT2 nanocomposite under UV light irradiation.

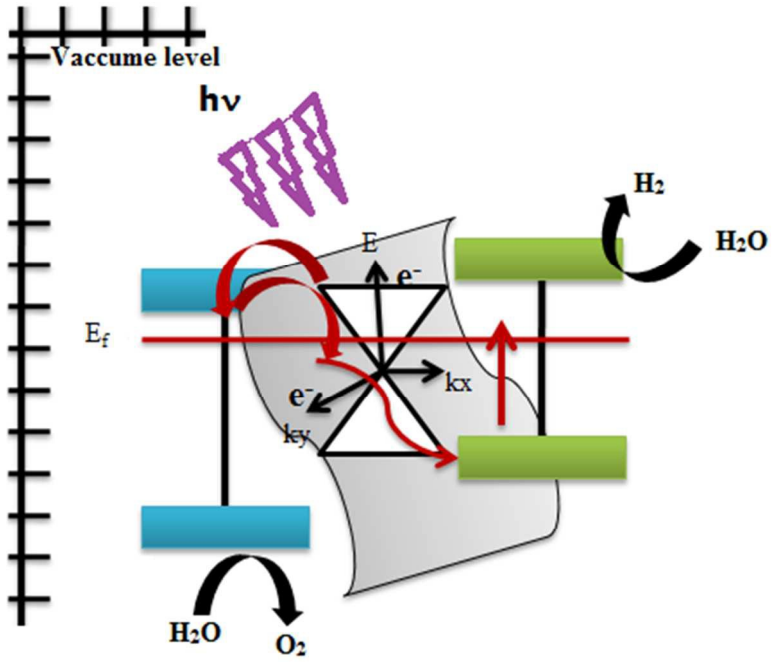

Fig. 12. Mechanism for photocatalytic hydrogen production studies.